Astron. Astrophys. 348, 945–949 (1999)

ASTRONOMY AND ASTROPHYSICS

ISOCAM spectro-imaging of the H_2 rotational lines in the supernova remnant IC 443⋆

D. Cesarsky[1], P. Cox[1], G. Pineau des Forêts[2], E.F. van Dishoeck[3], F. Boulanger[1], and C.M. Wright[4]

[1] Institut d'Astrophysique Spatiale, Bât. 120, Université de Paris XI, F-91405 CEDEX Orsay, France
[2] DAEC, Observatoire de Paris, F-92195 Meudon Principal CEDEX, France
[3] Leiden Observatory, P.O. Box 9513, 2300 RA Leiden, The Netherlands
[4] School of Physics, University College, ADFA, UNSW, Canberra ACT 2600, Australia

Received 7 May 1999 / Accepted 23 June 1999

Abstract. We report spectro-imaging observations of the bright western ridge of the supernova remnant IC 443 obtained with the ISOCAM circular variable filter (CVF) on board the *Infrared Space Observatory (ISO)*. This ridge corresponds to a location where the interaction between the blast wave of the supernova and ambient molecular gas is amongst the strongest. The CVF data show that the 5 to 14 μm spectrum is dominated by the pure rotational lines of molecular hydrogen (v = 0–0, S(2) to S(8) transitions). At all positions along the ridge, the H_2 rotational lines are very strong with typical line fluxes of 10^{-4} to 10^{-3} erg s^{-1} cm^{-2} sr^{-1}. We compare the data to a new time-dependent shock model; the rotational line fluxes in IC 443 are reproduced within factors of 2 for evolutionary times between 1,000 and 2,000 years with a shock velocity of $\sim 30\,\mathrm{km\,s^{-1}}$ and a pre-shock density of $\sim 10^4\,\mathrm{cm^{-3}}$.

Key words: ISM: individual objects: IC 443 – ISM: supernova remnants – infrared: ISM: lines and bands – shock waves

1. Introduction

The supernova remnant IC 443 is a prime example of the interaction of a supernova blast wave with an ambient molecular cloud. On optical plates, IC 443 appears as an incomplete shell of filaments (Fig. 1) with a total extent of about 20 arcmin, i.e. $\sim 9\,\mathrm{pc}$ for an adopted distance of 1500 pc. The shock generated by the supernova explosion, that occurred $(4\text{–}13) \times 10^3$ years ago, encountered nearby molecular gas which is mainly found along a NW-SE direction across the face of the optical shell. IC 443 has been the subject of numerous studies from X-rays, visible, infrared to radio wavelengths (e.g. Mufson et al. 1986 and references therein). Studies of the interaction between the shock and the ambient molecular gas were done by observing molecular hydrogen in the rotational–vibrational transitions (Burton et al. 1988, 1990 – see Fig. 1 – and Richter et al. 1995a), in the pure rotational S(2) transition (Richter et al. 1995b), in other simple molecules such as CO and HCO^+ (e.g., van Dishoeck et al. 1993 and references therein) and in atomic carbon (Keene et al. 1996).

In this letter we report mapping results of the pure rotational lines of H_2 using the ISOCAM CVF over the western ridge of IC 443, a position corresponding to clump G in the nomenclature of Huang et al. (1986). The observations reveal the details of the structure and the physical conditions of the shocked molecular gas in IC 443 with a pixel field of view of $6''$ and at unprecedented sensitivity (mJy). The observed H_2 line fluxes are well predicted by a time-dependent shock model recently developed by Chièze et al. (1998) and Flower & Pineau des Forêts (1999).

2. Observations and data reduction

The observations were done in 1998 February with the ISOCAM CVF (Cesarsky et al. 1996). A pixel size of $6''$ was used, yielding a total field of view of $3' \times 3'$. Scans of the long-wavelength CVF were obtained: the LW-CVF2 from 13.53 to 9 μm and then the LW-CVF1 from 9 to 5.0 μm for a total of 115 wavelength steps; the resolving power is 40. Each wavelength was observed for 12.6 sec, i.e. six readouts at 2.1 sec, for a total observing time of some 30 minutes.

ISOCAM was pointed towards α = 06h 13m 41.0s and δ = 22° 33′ 10.4″ (coordinates B1950.0), a position corresponding to the center of the molecular clump G which is also a peak in the H_2 emission (Fig. 1).

The data reduction includes a new time dependent dark current correction (Biviano & Sauvage, in preparation) as well as a new correction procedure for the transients (Coulais & Abergel 1999). The photometric calibration was done using the calibration files applicable to the current release of the ISOCAM off-line processing software (V7.0); the absolute calibration is conservatively estimated to be on the order of 25%.

The zodiacal background was subtracted adopting the spectrum obtained by Reach et al. (1996; but note that the published data were reduced again using the same algorithms and calibra-

Send offprint requests to: P. Cox (cox@ias.fr)

⋆ Based on observations with ISO, an ESA project with instruments funded by ESA Member States (especially the PI countries: France, Germany, the Netherlands and the United Kingdom) and with the participation of ISAS and NASA.

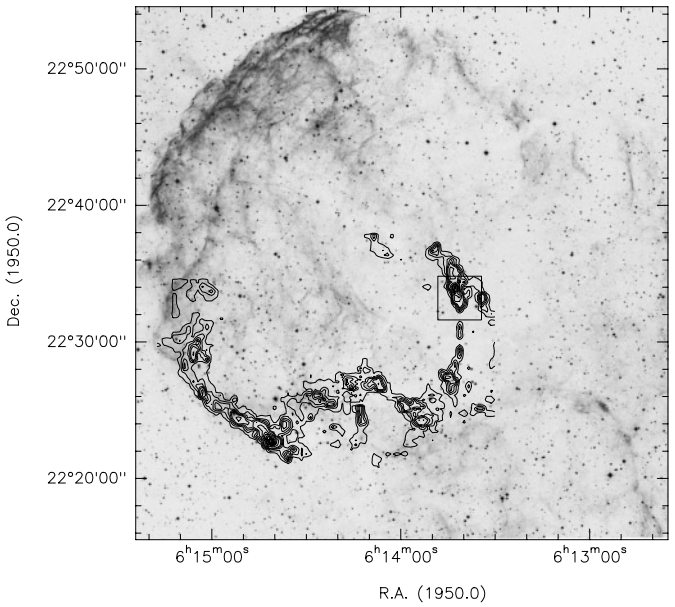

Fig. 1. The footprint of ISOCAM (box) depicted against the DSS image of the IC 443 supernova remnant together with the H_2 1–0S(1) emission (contours) from Burton et al. (1990).

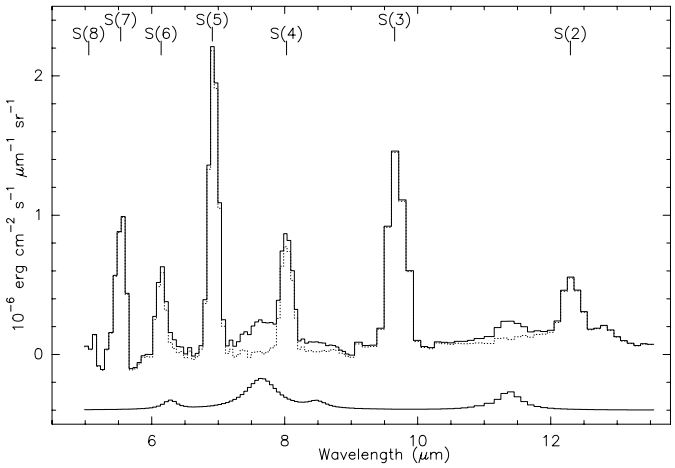

Fig. 2. IC443 mean CVF spectrum, i.e. integrated over the observed field, before (solid line) and after (dotted line) subtraction of the dust bands spectrum which is shown at the bottom of the figure at true scale but shifted down by $4\,10^{-7}$ erg s^{-1} cm^{-2} μm^{-1} sr^{-1}. The rotational lines of molecular hydrogen are labeled.

tion files as applied to the current data) with a scaling factor of 0.7.

The flux of the H_2 lines was obtained by numerical integration under the line profile, after subtracting a linear baseline defined by several points at either side of the line profile; the line fluxes thus obtained are independent of the assumed zodiacal background. We estimate the statistic uncertainty of the numerical integration by applying the same integration algorithm to regions of the spectrum devoid of any spectral emission; we consistently obtain an rms noise of some $2\,10^{-5}$ erg s^{-1} cm^{-2} sr^{-1}.

3. Results

The 5 to 14 μm spectrum of the molecular clump G in IC 443 is dominated by the series of the pure ($v = 0 - 0$) rotational lines of molecular hydrogen from the S(2) to the S(8) transitions (Fig. 2). In particular, there is no indication of any atomic fine structure line. At low level intensity, the This set of dust emission bands from 6.2 to 11.3 μm is clearly present, including the 12.7 μm band. Note that the relative strength of the dust bands is typical of that of the ISM (Boulanger 1998), suggesting that a possible contribution from the [Ne II] line at 12.8 μm is negligeable. This dust emission has comparable intensities over the entire ISOCAM field, i.e. a few MJy sr^{-1}, which is similar to the intensities measured in diffuse regions of the Ophiucus cloud. An image in one of the dust bands, e.g. 7.7 μm, does not show any structure correlated with the molecular filament. Using the trend between the band intensity and the UV radiation field shown by Boulanger (1998), we find that the excitation of the dust bands is commensurable with a radiation field $G \sim 10 \times G_0$. The dust bands are probably unrelated to the supernova remnant and more likely mixed with the interstellar gas along the 1.5 kpc line of sight toward IC 443. Although very faint, the 7.7 and 6.2 μm dust bands contaminate the S(4) and S(6) H_2 lines. We have fitted Lorentzians to the dust bands (Boulanger et al. 1998) and removed the resulting mean dust band spectrum from each individual CVF spectrum prior to performing the numerical integrations.

Fig. 3 shows the total emission of the H_2 lines between 5 and 13.5 μm, i.e. the sum of the S(2) to S(7) lines, together with the integrated line intensity of the S(2) and S(7) transitions (top panels). The H_2 emission is found along a ridge of about $30'' \times 80''$ (0.25 pc$\times$0.65 pc) running SW to NE, a structure which is comparable to that seen in CO or HCO^+ (van Dishoeck et al. 1993, Tauber et al. 1994). The higher spatial resolution of the ISOCAM data clearly reveal a series of knots sitting on a plateau. The H_2 knots are very bright with peak values of a few 10^{-3} erg s^{-1} cm^{-2} sr^{-1} (Table 1). The eastern side of the molecular ridge, facing the origin of the supernova explosion, appears sharper than the opposite side where weak emission is found extending westwards.

4. Discussion

Altogether there are about 130 pixels that show H_2 emission with intensities above the $10\,\sigma$ level, i.e. $> 2\,10^{-4}$ erg s^{-1} cm^{-2} sr^{-1} for all the six rotational transitions S(2) to S(7). This fact allows the construction of as many H_2 excitation diagrams which plot the logarithm of the column density, corrected for statistical weight, in the upper level of each H_2 transition vs. the energy of that level, E_u. When calculating the column densities, we corrected the observed line fluxes for extinction, using a screen model and the extinction curve from Draine & Lee (1984). Peak A corresponds to a position studied by Moorhouse et al. (1991) and Richter et al. (1995a – their Position 3). Moorhouse et al. derived an extinction of $A_{2.12\ \mu m}$ = 0.6 mag., whereas Richter et al. estimated a some-

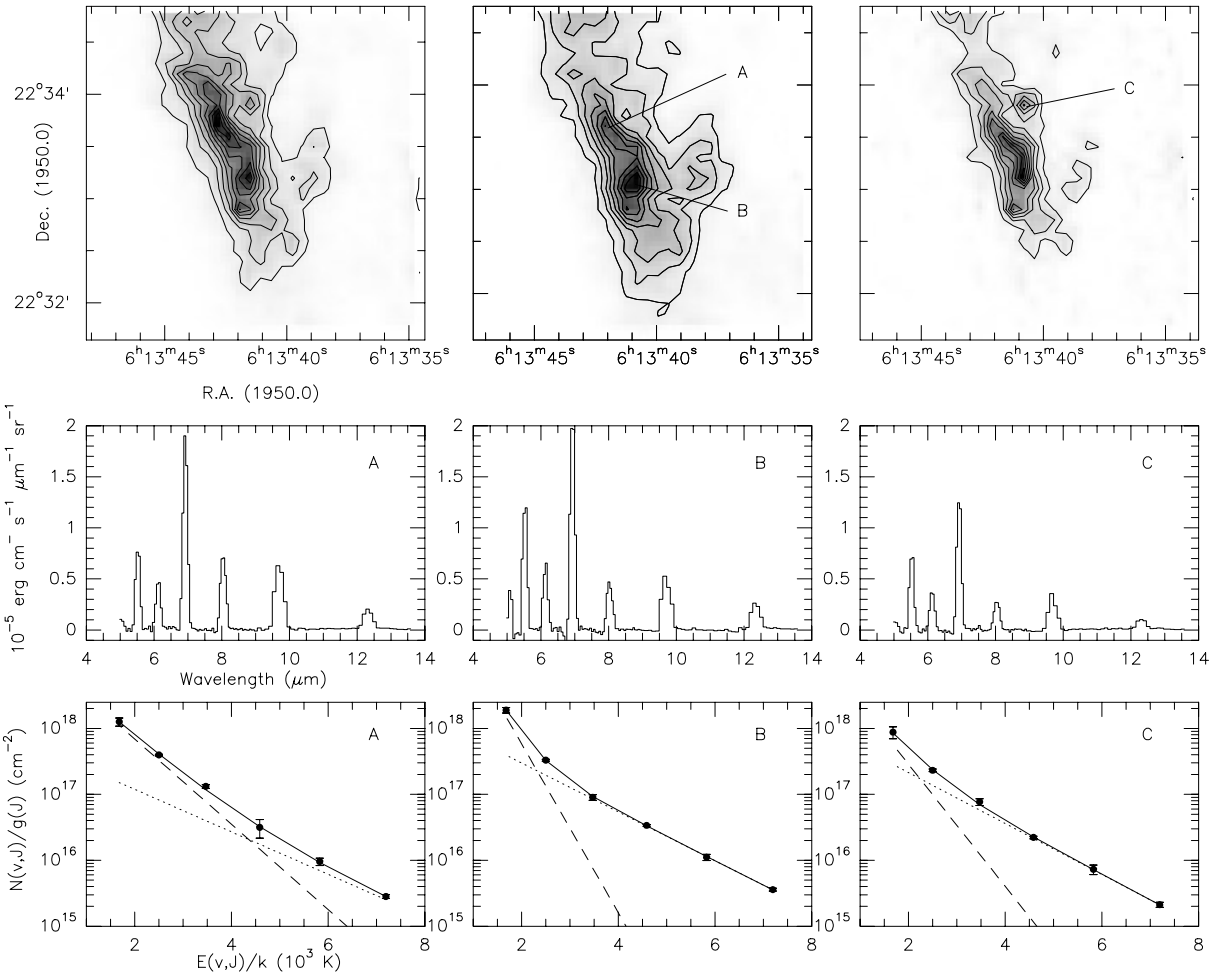

Fig. 3. The distribution of the emission of the S(2) to S(7) H_2 lines towards Clump G in IC 443 (upper left panel). The next top panels show the emission in the S(2) and S(7) H_2 lines. Contours are drawn at the 10%, 20%, etc. level. The corresponding peak strengths are 8.1 10^{-3}, 7.9 10^{-4} and 2.2 10^{-3} erg s^{-1} cm^{-2} sr^{-1} from left to right. The middle panels show the ISOCAM CVF spectra towards the three emission peaks A, B, and C. The lower panels present the excitation diagrams after correcting for an extinction of $A_{2.12}\ \mu\mathrm{m} = 0.6\,\mathrm{mag}$. Note that the spectra correspond to one pixel whereas the excitation diagrams have been built from a 3×3 pixel box car smoothed data. Each excitation diagram has been fitted with a two-component model involving 'warm' (dashed line) and 'hot' (dotted line) H_2. The full lines represent the sum of both H_2 components – see text and Table 1 for details.

what higher value ($\sim$ 1 mag.). We adopted the former value (see dereddening factors in Table 1). The middle and bottom panels in Fig. 3 present the CVF spectra and the corresponding excitation diagrams of the three emission peaks labeled A, B, C. The statistical weights used in Fig. 3 include a factor of 3 for ortho-H_2 and 1 for para-H_2.

The excitation diagrams for Peaks A, B, and C show that a single excitation temperature does not reproduce the H_2 lines observed in IC 443 and that emission from gas with a range of temperatures is required. The results of a simple LTE two-component H_2 model are shown in Fig. 3: a 'warm' H_2 component with an excitation temperature of ~ 500 K and typical column densities in between 10^{20} and 10^{21} cm^{-2}, and a 'hot' H_2 component with $T_{ex} \sim 1200$ K and N_{H_2} a few 10^{19} cm^{-2} (Table 1). The parameters of the 'warm' component are determined almost entirely by the intensities of the S(2) and S(3) lines and the 'hot' component dominates the H_2 transitions S(4) to S(7). Although the evidence for a 'warm' component is very strong, the ISOCAM data only poorly constrain its properties because of the lack of measurement of the S(1) and S(0) H_2 transitions. Furthermore, the uncertainty in the extinction correction (especially for the S(3) line whose position coincides with the peak of the silicate 9.7 μm band) introduces an additional uncertainty in the temperature determination. Using different extinction laws and adopting values for $A_{2.12}\ \mu$m between 0.5 and 1 mag., we derive typical uncertainties of ± 100 and ± 250 K for the warm and the hot components, respectively.

ISO spectroscopy of regions where shocks dominate the excitation has revealed that the shocked gas has a range of temperatures from a few 100 K to several 1000 K: Cepheus A (Wright et al. 1996), Orion (Rosenthal et al. 1999) and bipolar outflows (Cabrit et al. 1999). The H_2 lines cannot be explained by a single shock model and combinations of J- and/or C-type shocks with different velocities and pre-shock densities have been in-

Table 1. Line fluxes and derived parameters from the model fits – see text

H_2 Transition	S(2)	S(3)	S(4)	S(5)	S(6)	S(7)	Model fit			
Wavelength [μm]	12.28	9.66	8.02	6.91	6.11	5.51	Warm Component		Hot Component	
Dereddening factor[1]	1.16	1.42	1.13	1.07	1.08	1.09	T	N_{H_2}	T	N_{H_2}
Peak identification	Observed line flux [10^{-4} erg s^{-1} cm^{-2} sr^{-1}]						[K]	[10^{20} cm^{-2}]	[K]	[10^{20} cm^{-2}]
A	3.7	14.3	7.7	17.6	4.4	8.3	657	2.2	1288	0.22
B	5.1	11.9	5.3	18.9	5.1	10.3	330	19.7	1172	0.48
C	2.4	8.4	4.5	12.4	3.3	6.2	446	2.6	1115	0.37

[1] $10^{0.4\,A_\lambda}$ adopting the extinction curve of Draine & Lee (1984) and $A_{2.12\ \mu m} = 0.6$ mag.

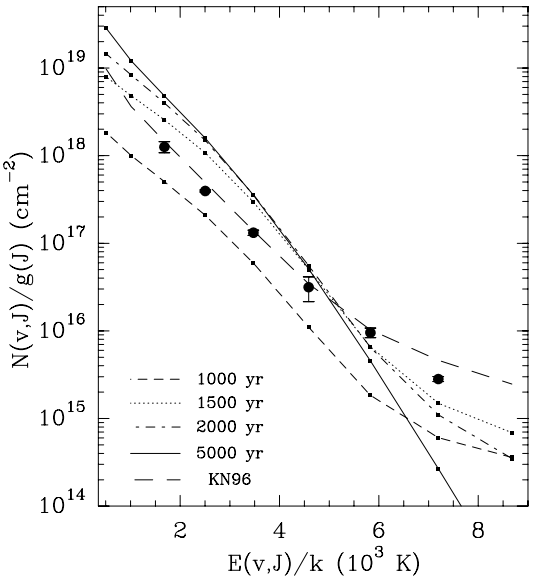

Fig. 4. The excitation diagram for Peak A (filled circles) compared to the predictions of the time-dependent shock model of Chièze et al. (1998) with a pre-shock density of $10^4\,\mathrm{cm}^{-3}$, a shock velocity of $30\,\mathrm{km\,s}^{-1}$ and four evolutionary times. The long-dashed curve labelled (KN96) presents the predictions of a model with two C-shocks from Kaufman & Neufeld (1996) – see text.

voked to account for the observed line fluxes. Similar conclusions have been reached for IC 443. Based on an analysis of the [O I] 63 μm fine structure line and near-infrared H_2 lines, Burton et al. (1990) concluded that the infrared line emission of IC 443 can only be modeled as a slow (10–20 $\mathrm{km\,s}^{-1}$), partially dissociating J shock where the oxygen chemistry is suppressed, i.e. the cooling is dominated by [O I] emission and not by H_2O cooling – see also Richter et al. (1995a, 1995b). Far-infrared spectroscopy obtained with ISO on IC 443 confirms these conclusions and will be discussed in a forthcoming paper.

Following the interpretation of Wright et al. (1996) for the shocked H_2 gas in Cepheus A, the H_2 lines in IC 443 can be fit by a combination of two C-shocks from the models of Kaufman & Neufeld (1996). A good match to the data towards Peak A is obtained combining a first shock with a pre-shock density of $10^4\,\mathrm{cm}^{-3}$, a velocity of $20\,\mathrm{kms}^{-1}$ and a covering factor Φ of 0.85 with a second shock of $10^6\,\mathrm{cm}^{-3}$, $35\,\mathrm{kms}^{-1}$ and Φ of 0.008 (see Fig. 4). Such a steady-state model requires at least two C-shocks with a set of 3 free parameters and relatively high pre-shock densities for the high velocity component.

Recently, Chièze et al. (1998) pointed out that the intensities of the ro-vibrational H_2 lines are sensitive to the temporal evolution of a shock wave. In many astrophysical situations, shock waves are unlikely to have reached steady-state which occurs at approximately 10^4 yr. At times scales of a few 10^3 yr, the shocked gas may show both C- and J-type characteristics: within the C-shock, a J-type shock is established heating a small fraction of the gas to high temperatures (Flower & Pineau des Forêts 1999). In the case of IC 443, the typical size of the molecular clump G is $\leq 20''$, i.e. $\leq 2 \times 10^{17}$ cm, but some of the molecular clumps have typical sizes of about a few arcsecs (Richter et al. 1995a). For a shock velocity of 20–30 kms^{-1}, the crossing time of the shock wave is thus ≤ 2500–4000 yr indicating that the shock wave in clump G is not in steady-state.

Fig. 4 shows the predictions of the time-dependent shock model for an observation along the direction of the shock propagation. The model results are given for four evolutionary times with the following parameters: pre-shock gas density $n_H = 10^4\,\mathrm{cm}^{-3}$, shock velocity $v_s = 30\,\mathrm{kms}^{-1}$, magnetic field strength $B = 100\,\mu$G and ortho-to-para ratio of 3. The filling factor in this model is equal to 1. A smaller filling factor could be compensated by a larger line of sight path across the shocked H_2 gas for a non face-on shock. The post-shock densities are 10^5–$10^6\,\mathrm{cm}^{-3}$ comparable with the values derived by van Dishoeck et al. (1993). The agreement between the model predictions and the observations is best for earlier epochs when the C-shock intermediate times, i.e. ≤ 2000 yr. At earlier epochs when the J-shock dominates, the low excitation H_2 lines are too weak. And after 5000 yr, excitation H_2 lines are too when the C-shock steady-state is reached, the higher excitation H_2 lines (above 10^4 K) are much too weak. In between, the intensities of the H_2 rotational lines are predicted within factors of 2 and the coexistence of the 'hot' and 'warm' H_2 components is well explained within a single model. Models with other parameters (e.g., $n_H = 3 \times 10^3\,\mathrm{cm}^{-3}$, $v_s = 35\,\mathrm{kms}^{-1}$) provide less good fits. The best fits are obtained for early evolutionary times ($\sim$ 1000–2000 years) and densities of $\sim 10^4\,\mathrm{cm}^{-3}$ with shock velocities $v_s = 30$–$40\,\mathrm{kms}^{-1}$. Higher shock velocities will predict too large intensities for the high-excitation H_2 lines.

The agreement between these time-dependent model predictions and the data of IC 443 is very encouraging in view of some of the simplistic underlying assumptions. In particular, the

assumed geometry (plane parallel) is oversimplified and does not describe the molecular filament which is seen edge-on and consists of numerous small clumps. Clearly a more thorough study should be done to explore the entire parameter space of the model and compare the predictions with additional data available on IC 443.

In the model, the S(2) to S(7) lines account for about 70% of the luminosity in all the H_2 lines. At peak A, the measured S(2) to S(7) flux is $\sim 4.6 \times 10^{-12}$ erg s^{-1} cm^{-2} ($\sim 0.4\,L_\odot$) and, according to the model, the H_2 lines alone would thus carry $\sim 0.6 L_\odot$. Towards clump G, the S(3) and S(2) H_2 lines account for almost the entire IRAS 12 μm-band emission. The mean value of these lines in that band is 5.4 MJy sr^{-1} comparable to the IRAS peak value, i.e. 6 MJy sr^{-1} (e.g., Oliva et al. 1999). Similarly, the IRAS 25 μm-band could also be due to H_2 line emission. The model predictions (Fig. 4) for the S(0) and S(1) line fluxes (at an evolutionary time of 2000 years) are $1.2\,10^{-5}$ and $7.7\,10^{-4}$ erg s^{-1} cm^{-2} sr^{-1}, respectively. Taking into account the 20% transmission at 17.03 μm of the IRAS 25 μm band, the strong S(1) line would thus contribute ~ 4 MJy sr^{-1} at 25 μm, which is comparable to the measured 25 μm IRAS flux at Peak A (~ 4.5 MJy sr^{-1}, e.g. Oliva et al. 1999). These results strongly suggest that the excitation of the gas in IC 443 is entirely collisional.

Finally, Oliva et al. (1999) found towards the optical filaments of IC 443, which trace the low density atomic gas, that most of the 12 and 25 μm IRAS fluxes is accounted for by ionized line emission (mainly [Ne II] and [Fe II]). Our results show that this conclusion cannot be generalised towards the molecular hydrogen ring (Fig. 1) where the dense molecular gas essentially cools via the H_2 lines in the near- and mid-infrared and via the [O I] emission line in the far-infrared.

Acknowledgements. Michael Burton is kindly thanked for providing his H_2 map of IC 443.

References

Boulanger F., 1998, In: Yun J.L., Liseau R. (eds.) Star Formation with ISO. ASP Conference Series, vol. 132, p. 15
Boulanger F., Boissel P., Cesarsky D., Ryter C., 1998, A&A 339, 194
Burton M.G., Geballe T.R., Brand P.W.J.L., Webster A.S., 1988, MNRAS 231, 617
Burton M.G., Hollenbach D.J., Haas M.R., Erickson E.F., 1990, ApJ 355, 197
Cabrit S., Bontemps S., Lagage P.O., et al., 1999, In: Cox P., Kessler M.F. (eds.) The Universe as seen by ISO. ESA proc., in press
Cesarsky C., Abergel A., Agnèse P., et al., 1996, A&A 315, L32
Chièze J.-P., Pineau des Forêts G., Flower D.R., 1998, MNRAS 295, 672
Coulais A., Abergel A., 1999, In: Cox P., Kessler M.F. (eds.) The Universe as seen by ISO. ESA proc., in press
Draine B.T., Lee H.M., 1984, ApJ 285, 89
Flower D.R., Pineau des Forêts G., 1999, MNRAS, in press
Huang Y.-L., Dickman R.L., Snell R.L., 1986, ApJ 302, L63
Kaufman M.J., Neufeld D.A., 1996, ApJ 456, 611
Keene J., Phillips T.G., van Dishoeck E.F., 1996, In: Latter W.B., et al. (eds.) CO: Twenty-Five Years of Millimeter-Wave Spectroscopy. IAU Symp. 170, Kluwer, p. 382
Moorhouse A., Brand P.W.J.L., Geballe T.R., Burton M.G., 1991, MNRAS 253, 662
Mufson S.L., McCollough M.L., Dickel, et al., 1986, AJ 92, 1349
Oliva E., Lutz D., Dapratz S., Moorwood A.F.M., 1999, A&A 341, L75
Reach W.T., Abergel A., Boulanger F. et al., 1996, A&A 315, L381
Richter M.J., Graham J.R., Wright G.S., 1995a, ApJ 454, 277
Richter M.J., Graham J.R., Wright G.S., Kelly D.M., Lacy J.H., 1995b, ApJ 449, L83
Rosenthal D., Bertoldi F., Dapratz S., Timmermann R., 1999, In: Cox P., Kessler M.F. (eds.) The Universe as seen by ISO. ESA proc., in press
Tauber J.A., Snell R.L., Dickman R.L., Ziurys L.M., 1994, ApJ 421, 570
van Dishoeck E.F., Jansen D.J., Phillips T.G., 1993, A&A 279, 541
Wright C.M., Dapratz S., Timmermann R., et al., 1996, A&A 315, L301